Draft version December 8, 2017
Typeset using LaTeX **twocolumn** style in AASTeX61

THE ROTATION AND CHROMOSPHERIC ACTIVITY OF THE SOLAR-TYPE STARS IN THE OPEN CLUSTER M67

Mark S. Giampapa,[1,2] Axel Brandenburg,[3,4,5,6] Ann Marie Cody,[7] Brian A. Skiff,[8] and Jeffrey C. Hall[8]

[1] *National Solar Observatory, 950 N. Cherry Avenue, Tucson, AZ 85719, USA. The National Solar Observatory is operated by AURA under a cooperative agreement with the National Science Foundation.*
[2] *Visiting astronomer, Kitt Peak National Observatory, National Optical Astronomy Observatory, which is operated by the Association of Universities for Research in Astronomy (AURA) under a cooperative agreement with the National Science Foundation.*
[3] *Laboratory for Atmospheric and Space Physics, University of Colorado, Boulder, CO 80303, USA*
[4] *JILA and Department of Astrophysical and Planetary Sciences, University of Colorado, Boulder, CO 80303, USA*
[5] *Nordita, KTH Royal Institute of Technology and Stockholm University, Roslagstullsbacken 23, SE-10691 Stockholm, Sweden*
[6] *Department of Astronomy, AlbaNova University Center, Stockholm University, SE-10691 Stockholm, Sweden*
[7] *NASA Ames Research Center, Moffett Field, CA 94035, USA*
[8] *Lowell Observatory,1400 W Mars Hill Rd, Flagstaff, AZ 86001, USA*

(Received December 8, 2017; Revised ; Accepted)

Submitted to ApJ

ABSTRACT

We report the results of a program to measure rotation periods and chromospheric activity in solar-type members of the approximately solar-age and solar-metallicity open cluster, M67. We utilize *Kepler*/*K*2 data from *Campaign 5* along with contemporaneous spectroscopic observations of the Ca II H and K resonance lines as obtained with the 3.5-m WIYN telescope on Kitt Peak in conjunction with its Hydra multi-object spectrograph. We find for the solar-type stars in our sample that are classified as single members and that also exhibit rotational modulation of their light curves a mean rotation period of 23.0 days with a standard deviation for the sample of 2.7 days. With few exceptions, we do not detect solar-like rotation periods of 26 days or longer in the *K*2 data. Among the binaries with a solar-type primary in our sample, we find a faster mean rotation period of 15.4 ± 8.5 days. A general decline in chromospheric activity with increasing rotation period is present though with considerable scatter among the single members with rotation periods greater than about 19 days. The single solar-type M67 stars exhibit a correlation of activity with Rossby number that is opposite to that seen in the inhomogeneous (in age and metallicity) sample of field stars from the Mt. Wilson HK Survey. This unconventional behavior was theoretically predicted for stars characterized by Rossby number (the ratio of rotation period to convective turnover time) exceeding that of the Sun. Such stars are expected to have antisolar differential rotation, but with an increased angular velocity contrast between rapidly rotating poles and a slow equator. We also find that single solar-type members warmer than the Sun tend to have enhanced chromospheric emission than would otherwise be predicted by empirical relations for chromospheric decay combined with rotational evolution models. Finally, we estimate stellar ages based on gyrochronology relations and age-activity correlations, respectively, determining a mean chromospheric age of 4.5 ± 1.9 Gyr and a mean gyroage of 4.2 ± 1.0 Gyr. We discuss these methods for stellar age determination particularly in the context of their applicability for identifying stars in the field with ages similar to that of the Sun.

Keywords: open clusters and associations: individual (M67) — stars: solar-type — stars: activity — stars: rotation — Sun: activity

Corresponding author: Mark Giampapa
giampapa@nso.edu

1. INTRODUCTION

The solar-age and solar-metallicity open cluster, M67, is a benchmark cluster for understanding stellar evolution and the nature of solar-type stars. A particular focus of investigations of M67 has been studies of the comparative properties of the Sun and the solar-type members of this cluster. In this context, Giampapa et al. (2006, hereafter Paper I) conducted a survey of chromospheric activity of the solar counterparts in M67 based on spectroscopic observations of the emission cores of the Ca II resonance lines, which are manifestations of magnetic activity in the Sun and late-type stars (Eberhard & Schwarzschild 1913; Wilson 1966; Kraft 1967). Since that time a number of other studies have been published that are relevant to topics that will be discussed in this work. These include the identification of solar twins in M67 through a comparison of the photospheric features in their spectra as obtained at echelle resolutions with the same lines in the solar spectrum (Önehag et al. 2011); additional approaches to refining the estimated age of M67 (Yadav et al. 2008; Sarajedini et al. 2009; Bellini et al. 2010; Önehag et al. 2011); measurements of projected rotational velocities for a small sample of solar-type stars (Reiners & Giampapa 2009); an extensive radial velocity study to confirm membership and extend the list of known binary systems (Geller et al. 2015); and, the discovery of exoplanet systems, including a planet hosted by the solar twin S770 (Brucalassi et al. 2016).

The repurposed *Kepler* mission, referred to as *K*2 (Howell et al. 2014), enabled the acquisition of nearly continuous photometry of a region on the sky that included M67 during the $\sim$ 76-day duration of *Campaign 5*. This program yielded data of unprecedented photometric precision for M67 that allows us to examine the nature of broadband variability in the solar-type members. The specific objectives of our *K*2 Guest Observer program are to gain insights on the relationship between magnetic activity and rotation and, hence, angular momentum evolution at solar age. Therefore, in support of our *K*2 program we also obtained contemporaneous spectroscopic observations of the Ca II H and K resonance lines utilizing the WIYN 3.5-m telescope[1] on Kitt Peak in conjunction with its *Hydra* multiobject spectrograph. Both Barnes et al. (2016) and Gonzalez (2016b) reported rotation periods for main sequence, late-type stars in M67 based on the publicly available *K*2 *Campaign* 5 data, each examining their respective results in the context of gyrochronology. With little overlap between our sample of solar-type cluster members and the stars considered by Barnes et al. (2016) and Gonzalez (2016b), respectively, we extend these previous investigations through a primary focus on rotation and magnetic field-related activity at solar age.

A salient result of Paper I was the finding of a significant overlap between the distribution of chromospheric H and K strengths in the M67 solar-type stars and the cycle-modulated distribution of H and K exhibited by the Sun seen as a star. However, about 28% of the M67 stars had H and K chromospheric emission outside of the solar cycle distribution, either in excess of solar maximum levels or less than that of solar minimum. In view of these past results, it became compelling to obtain H and K spectra once again that were contemporaneous with the *K*2 photometry so that (1) the correlation, if any, between the visible band variations recorded by *K*2 with the current levels of chromospheric H and K emission could be examined, and (2) the distribution of H and K and its range of variation on the cycle-like time scale of a decade for the ensemble and for individual solar-type members can be compared with previous results. Unavailable at the time of the original M67 H and K survey, rotation periods, inferred herein from the *K*2 data, enable us to investigate the nature of the rotation-activity relationship at solar age for a homogeneous sample of solar-type stars. The results may then be compared to the form of the rotation-activity relation based on inhomogeneous stellar samples (in age and metallicity), such as that for field stars in the solar neighborhood based on the Mt. Wilson survey data (Baliunas et al. 1995; Noyes et al. 1984). Finally, the relationships between rotation period, chromospheric activity and age, and the implied age for M67 from gyrochronology relations (Barnes 2010) and activity-age correlations (Mamajek & Hillenbrand 2008), respectively, can be investigated and compared with the estimated age for M67 as deduced from other standard approaches primarily based on isochrones and main-sequence fitting (e.g., Sarajedini et al. 2009).

In §2 we discuss our analysis of the *K*2 photometric time series. In §3 we describe our ground-based H and K observations including their reduction and calibration to chromospheric emission fluxes. We give in §4 the resulting relationship between rotation and activity in the solar-type stars in M67 as well as the apparent age distributions based on, respectively, rotation periods and the distribution of chromospheric activity in the sample. We discuss the results in §5 and present our conclusions in §6 along with our envisaged directions for further work.

[1] The WIYN Observatory is a joint facility of the University of Wisconsin-Madison, Indiana University, the National Optical Astronomy Observatory and the University of Missouri.

2. REDUCTION AND ANALYSIS OF THE $K2$ PHOTOMETRIC TIME SERIES

We adopt the same photometric criteria as in Paper I for the selection of targets for our $K2$ *Cycle* 1 Guest Observer program, namely a range of apparent brightness of $14 \leq V < 15$ and intrinsic color of $0.58 \leq (B-V) \leq 0.78$, where we differ slightly from Paper I in the adoption of the more recent value of $E(B-V) = 0.041$ for the color excess in M67 (Taylor 2007). To the extent possible, our target selection focused on objects observed in Paper I.

The $K2$ data were obtained in *Campaign* 5 during the $\sim$ 76 day period from 27 April 2015 10 July 2015. We utilized long-cadence data, that is, a time series of approximately 1800 second integrations for each target. A detrending code (Aigrain et al. 2016) was applied to remove pointing systematics and identify outliers. The processing included a re-centroiding at the position of each target thus yielding light curves based on 1-pixel, 2-pixel, 3-pixel and 4-pixel apertures. We adopted the 4-pixel aperture light curves for our analysis and retained only those points with quality flags of mflag = 0 in order to minimize the effects of any instrumental effects (following Gonzalez 2016a; Barnes et al. 2016). Our emphasis on the 4-pixel aperture data is based on their higher signal-to-noise ratio and the appearance of a strong systematic in the 1-pixel – 3-pixel-aperture data in the form of a strongly dominant peak in the power spectrum for each target in the $\sim$ 30 – 33 day range and sometimes at longer periods in the 40 – 50 day range. This peak declined in importance and was not nearly as evident in the 4-pixel data though exceptions are present in some targets.

We detrended the K2 light curve with a low-order polynomial and searched for periodicities due to the rotational modulation of surface heterogeneities that, in the visible bandpass of *Kepler*, we expect to be due to starspots, in analogy to what we see in the Sun viewed as a star (Shapiro et al. 2016; Giampapa 2016). We applied a dual approach based on the application of algorithms to compute the Lomb-Scargle periodogram (Press & Rybicki 1989) supported by the construction of a wavelet contour map (Torrence & Compo 1998). After detrending we excluded points that deviated more than 4σ from the mean of the light curve to further exclude outliers. We then applied a split cosine bell tapering to the beginning and the end of each light curve, comprising a total of 15% of the data points, in order to suppress leakage in the periodogram (Bloomfield 1976, pp. 80–94). We identified a significant peak in the periodogram with the rotation frequency if we also found support for the corresponding period in the wavelet contour map. If the wavelet map and the collapsed wavelet appeared to support the period measured in the Lomb-Scargle periodogram then we adopted this value as the rotation period of the star. The measured period is based on a Gaussian fit to the peak in the periodogram utilizing the *splot* routine in IRAF to identify the central frequency. We adopt for the error in the rotation period the standard deviation of the fitted Gaussian.

In some cases we could not measure a period either because the signal-to-noise ratios of the periodogram and the wavelet were each too low or the signal was dominated by underlying systematics. In the case of the latter, we had success with some objects in deducing a rotation period through the application of a novel approach. In particular, we constructed an average time series by adding together the normalized time series of the single, solar-type members present in our $K2$ data comprised of 33 objects. By so doing, the rotational signatures should be largely smeared out but any signal due to common instrument systematics retained. We then divided the time series of an individual object by this average time series in order to remove or at least suppress instrumental and other observational effects not intrinsic to the target. This approach was successful with some but not all objects that exhibited strong underlying systematics.

An example of the results of our $K2$ time series analysis for the single solar-type star, S958, is given in Figure 1. The collapsed wavelet and the computed Lomb-Scargle periodogram each exhibit a dominant power peak at a period of about 23.8 days. While a secondary peak appears near $\sim$ 13 – 14 days, the wavelet reveals that the $\sim$ 24 day period persists throughout the time series. In Figure 2 we illustrate the results of the same kind of analysis but for the active binary, S1452. Obvious periodic variability is present in the $K2$ time series for this SB1 member that is also characterized by relatively strong chromospheric emission (Table 1). Applying a Lomb-Scargle periodogram to its $K2$ time series reveals two peaks at high signal-to-noise ratios, suggestive of two distinct rotation frequencies at corresponding periods of about 4.35 days and 4.84 days, respectively. The computed wavelet also exhibits these periods with onsets at different times during the campaign, suggestive of the detection of differential rotation. However, we note that in work in progress, G. Basri has found that finite spot evolutionary lifetimes can give rise to a signal that mimics differential rotation. Applying his preliminary model to our time series for S1452 yields a single period of 4.56 days that is consistent with the data (Basri 2017, private communication). Interestingly, the collapsed wavelet also yields a single period at about

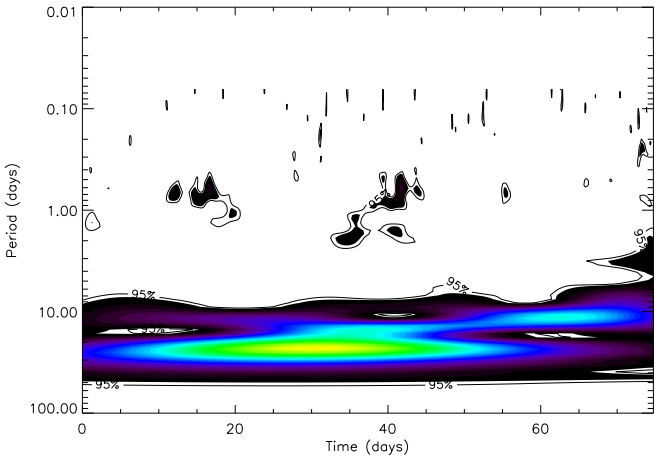

(a)

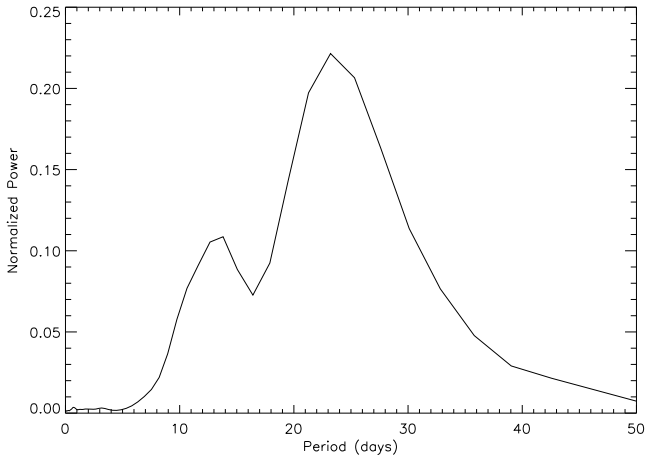

(b)

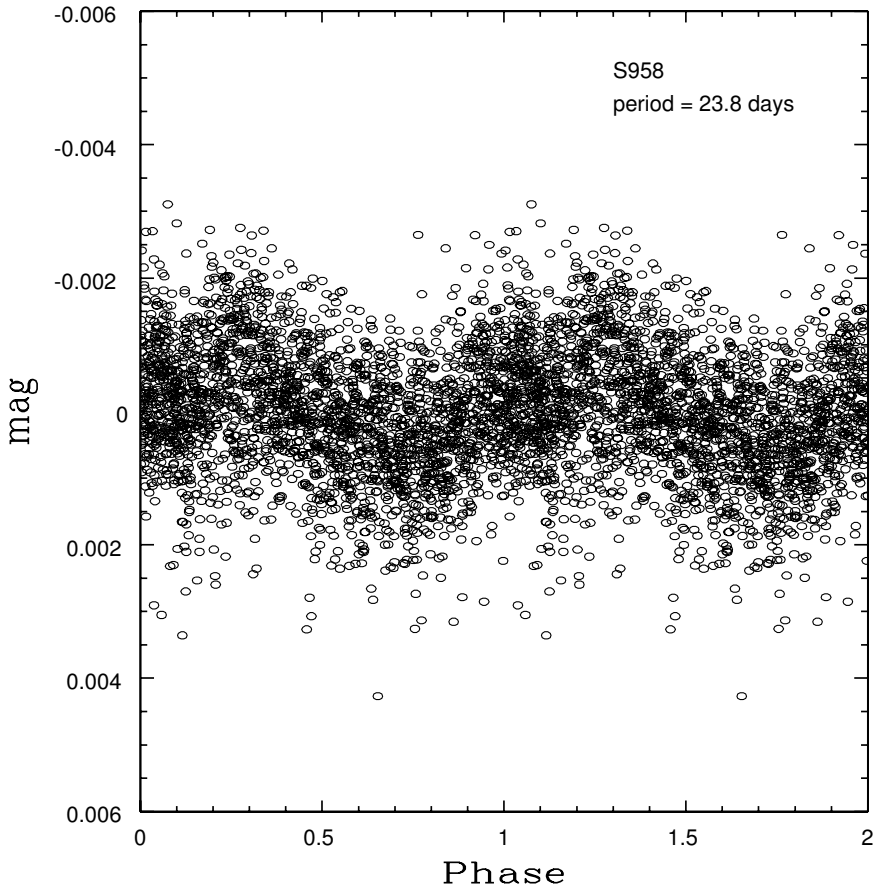

(c)

Figure 1. (a) The wavelet (period-time diagram) for S958. (b) The corresponding periodogram from the collapsed wavelet is displayed. (c) The phased light curve at the period given in Table 1.

4.56 days (Figure 2). We therefore adopt this value of the rotation period for the analysis herein.

We note, parenthetically, that Reiners & Giampapa (2009) measured a projected rotation velocity for S1452 of 4 ± 0.5 km s^{-1}. When combined with our rotation period measurement, and assuming a solar radius for S1452, yields an inclination to the line-of-sight of sin$i$ = 0.09. Therefore, it is unlikely there are observable transits of any exoplanets that may be present unless their orbits have high obliquities, such as is the case for the active K dwarf HAT-P-11 (Morris et al. 2017). Furthermore, a Jovian-mass planet would have to be within 1 AU of S1452 to exhibit a detectable radial velocity semi-amplitude greater than about 2.5 m s^{-1} (following Lovis & Fischer 2010).

3. REDUCTION AND CALIBRATION OF THE H AND K SPECTRA

We obtained spectra of 53 of our $K2$ targets utilizing the *Hydra* multifiber positioner in conjunction with the bench spectrograph and the 3.5-m WIYN telescope on Kitt Peak, Arizona, during UT 2016 January 27 – February 3, or approximately 6 months following the end of $K2$ *Campaign* 5. We utilized an identical instrument configuration to that of Paper I, namely, the bench-mounted spectrograph with the 1200 g mm^{-1} in second order, the 3-arcsecond-diameter blue fiber cables, a $CUSO_4$ blocking filter to suppress red leak, and the Simmons camera but with a STA1 CCD, which is the only difference from the survey in Paper I. In view of the limited time available to obtain spectra of high S/N ratio in the deep cores of the H & K lines, we adopted an observational strategy that included 4 × 3 binning of the CCD. This entire configuration yielded a spectral resolution of 0.91 Å ± 0.01 Å in the H and K region as compared to the 0.80 Å ± 0.03 Å resolution spectral resolution that characterized the multi-season program for the initial survey of Paper I. Therefore, in order to intercompare the current and previous HK index values from Paper I we applied an empirical correction of 11.5% to our HK flux measurements derived from a comparison of the mean values for a sample of the same stars as in Paper I. This correction is based on the reasonable assumption that the respective mean values for the two samples are stable for uncorrelated variations. Our methods for data reduction and for calibration to fluxes follows exactly that as given in Paper I. In particular, we applied empirical relations as a function of $(B-V)$ color given by Hall & Lockwood (1995) combined with our HK index values to estimate total fluxes in the 1 Å bandpass centered on the H and K lines for each stellar spectrum.

3.1. *Light curve variability and activity*

The availability of high-precision photometric light curves and activity measures enable us to examine the correlation between brightness variations and chromospheric activity. The Sun itself exhibits a direct correlation between its bolometric flux and activity cycle in the sense that as activity increases the Sun becomes brighter by an average of about 0.1% and fainter at solar minimum. On rotational time scales, the disk passage of sunspots causes diminutions in the range of 0.1% – 0.3% (for a comprehensive review of solar irradiance variability see Solanki & Unruh 2013). Utilizing *Solar Radiation and Climate Experiment* (SORCE) satellite data, specifically in the counterpart of the Kepler visible band of approximately ∼ 400 nm – 900nm, combined with SOLIS Integrated Sunlight Spectrometer (ISS) data for the 1 Å K line parameter time series available for the same days as the SORCE data, Giampapa (2016) finds that the K line data and brightness variations for the Sun as a star are uncorrelated on short time scales. Only during occasional periods coinciding with the disk passage of major spot complexes does a correlation between the K line parameter and the observed spot modulation in the SORCE "Kepler bandpass" appear, suggesting that flux variations in broad visible bandpasses are mostly independent of chromospheric activity in stars at solar-like levels of activity on time scales much less than an activity cycle time scale.

In the case of our sample of M67 solar-type stars, we calculate the standard deviation of our detrended light curves and compare this value with the activity index, $R'_{\rm HK}$, as illustrated in Figure 3. The sample is divided into those objects for which we are able to measure a rotation period and those that we do not detect rotational modulation of the $K2$ light curve. We see that the latter group appears to dominate at low, quiescent levels of $R'_{\rm HK}$ but can span a large range in standard deviation from about ∼ 0.1% to 0.8%. This is consistent with the above findings for the Sun as a star. The appearance of rotational modulation of the light curve depends on sustained departures from axial symmetry in the distribution of spots, which dominate variability in the visible band (Giampapa 2016). Therefore, at or near solar-like levels of activity the light curve variability is dominated by non-periodic, possibly stochastic variations. The light curves with measured rotation periods generally have values of σ ∼ 0.1% – 0.2% and tend to be more active than the Sun. The distribution in activity of these two groups is given in the histogram in Figure 3. At low-activity non-detections of rotational modulation predominate though there is considerable overlap between both groups. This is reflected in the mean values

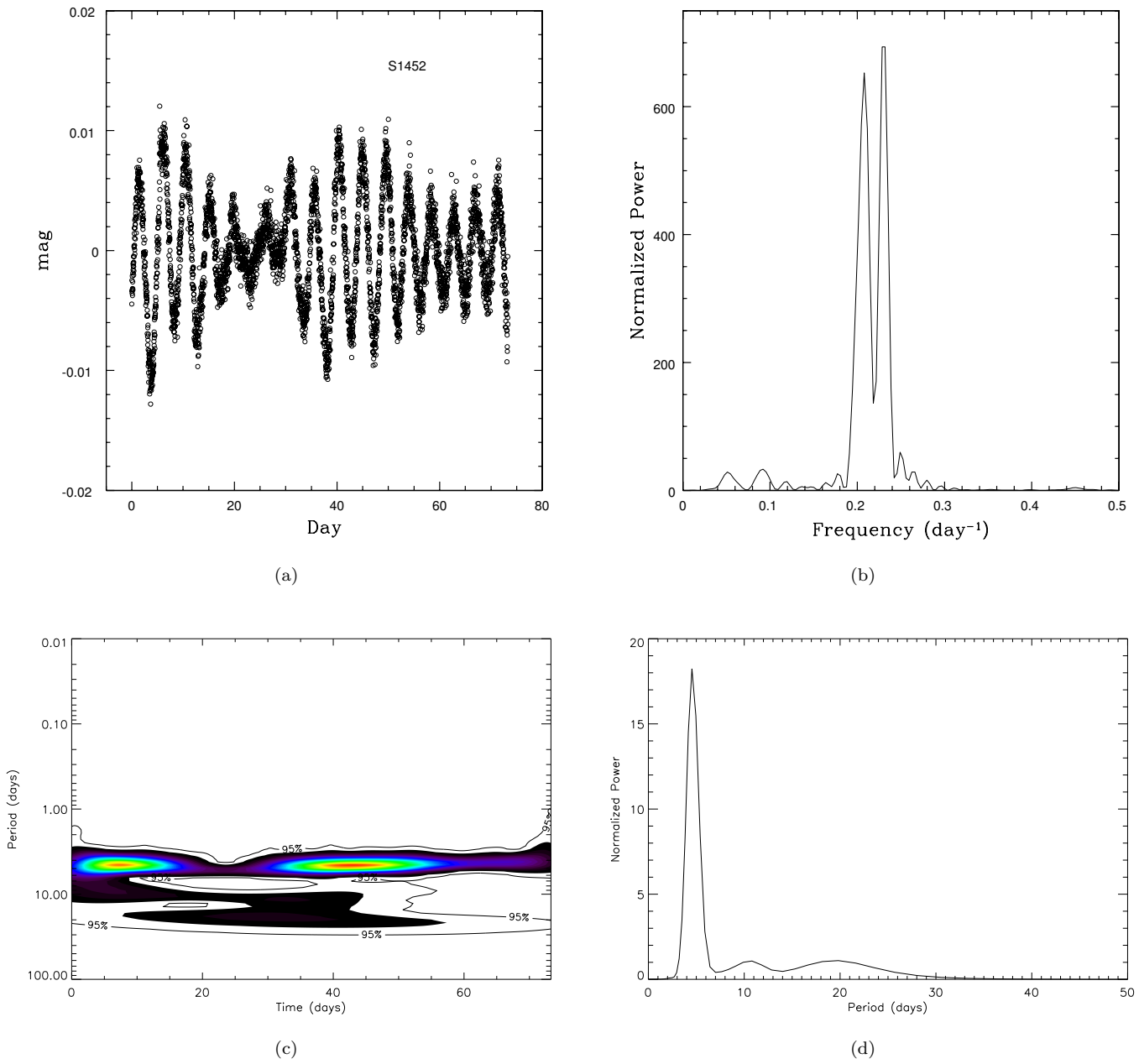

Figure 2. (a) The $K2$ time series for the chromospherically active M67 binary member S1452. (b) The Lomb-Scargle periodogram of the detrended time series exhibits two peaks at frequencies in the 4 – 5-day range. (c) The wavelet for the time series corroborates the occurrence of two apparent periods with onsets at different times during the $K2$ Campaign. (d) The collapsed wavelet is consistent with a single period at about 4.6 days.

of $R'_{\rm HK}$ where we find that those stars with measured rotation periods have mean $R'_{\rm HK} = 1.6 \times 10^{-5} \pm 6.2 \times 10^{-6}$ and those without periods a virtually indistinguishable mean of $R'_{\rm HK} = 1.5 \times 10^{-5} \pm 6.2 \times 10^{-6}$.

We also indicate the range of the same quantity for the Sun in Figure 3 deduced in the following manner. We utilized the absolute flux measurements obtained with the Spectral Irradiance Monitor (SIM) on board the SORCE satellite as obtained from 2003 April to 2011 May, corresponding to the descending phase from solar maximum and extending into the prolonged minimum of Cycle 23. The SORCE satellite is described by Rottman (2005) while Rottman (2006) gives the specifications for the SIM instrument. We utilized those SIM data that overlapped with the *Kepler* visible bandpass of approximately 400 nm – 900 nm. After detrending to eliminate

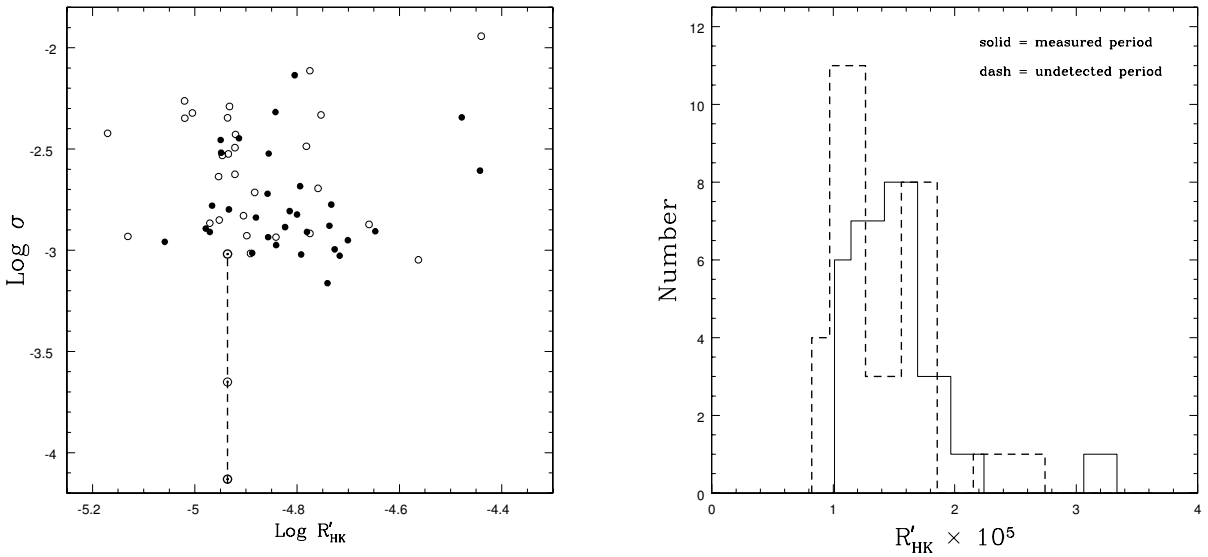

Figure 3. The standard deviation of the detrended $K2$ light curve for solar-type stars with (filled circles) and without (open circles) rotation period measurements (left panel) for both single and binary members. The range of this quantity for the Sun along with its mean value during a portion of Cycle 23 is indicated at the mean value of $R'_{\rm HK}$ adopted in this investigation. A histogram of the distribution with chromospheric activity index $R'_{\rm HK}$ for the sample considered herein with and without measured rotation periods (right panel). See text for a discussion.

relatively long period drifts we calculated the standard deviation in a 76-day running boxcar (i.e., the same duration as the $K2$ data), which yielded the range in the light-curve σ in the visible band for the Sun during this period in its cycle, as shown in Figure 3. It is evident that the maximum in the light-curve standard deviation for the Sun, which occurred during the descending phase from the maximum of Cycle 23 in these data, is near the minimum level of that for the M67 solar-type stars. We note that the mean value for the Sun shown in Figure 3 is weighted more near the minimum, likely reflecting the prolonged Cycle 23 minimum in activity. We recall from Paper I that the mean rms variation in HK index for the M67 solar-type stars was about 2.5 times greater than that for the Sun (from 1976 – 2004). Therefore, the comparison of the Sun with the variability of the M67 solar-type stars in Figure 3 is qualitatively consistent with this result to the extent that brightness changes and chromospheric variations are correlated in sunlike stars (e.g., Lockwood et al. 2007). The results in Figure 3 suggest that, in general, the Sun appears more photometrically quiescent than the solar-type stars in M67 or, in other words, nearly all the M67 solar-type stars are more variable photometrically than the Sun.

4. RESULTS

We provide in Table 1 a summary of our principal observational results, specifically the HK index and rotation periods for our sample of solar-type members of M67. In Table 2 we give derived parameters based on the adopted calibration relations (§2 and Paper I). In particular, in order to enable intercomparison among stars with different effective temperatures, apply age-activity calibrations in the literature and examine critical correlations with activity and age, we adopt the normalized parameter $R'_{\rm HK}$, defined as the total chromospheric flux in the Ca II H and K lines divided by the bolometric flux of the star (Linsky et al. 1979). As in Paper I, we derive this parameter by applying an empirical radiative equilibrium correction, given by Noyes et al. (1984) as a function of $(B-V)$ color, to the total H and K fluxes in the 1 Å bandpass. This yields the contribution of the chromospheric emission to the line flux in the core. The bolometric flux is based on the calibration of effective temperature with $(B-V)$ color determined by Hall & Lockwood (1995) for solar-type stars.

4.1. *Rotation and Activity in the Solar-Type Stars*

The relationship between rotation and activity in the single M67 solar-type stars based on the data in Table 2 is displayed in Figure 5. We confine ourselves to an analysis of the single stars in order to avoid additional complexities that binary systems entail. In particular, the most chromospherically active objects are binary systems with rotation periods less than 10 days. Apparently, rapid rotation can be prolonged in some binaries even in systems that are solar age. We see in Figure 5 that there is a general decline of the normalized activity parameter $R'_{\rm HK}$ with increasing rotation period though with considerable scatter at solar-like rotation periods

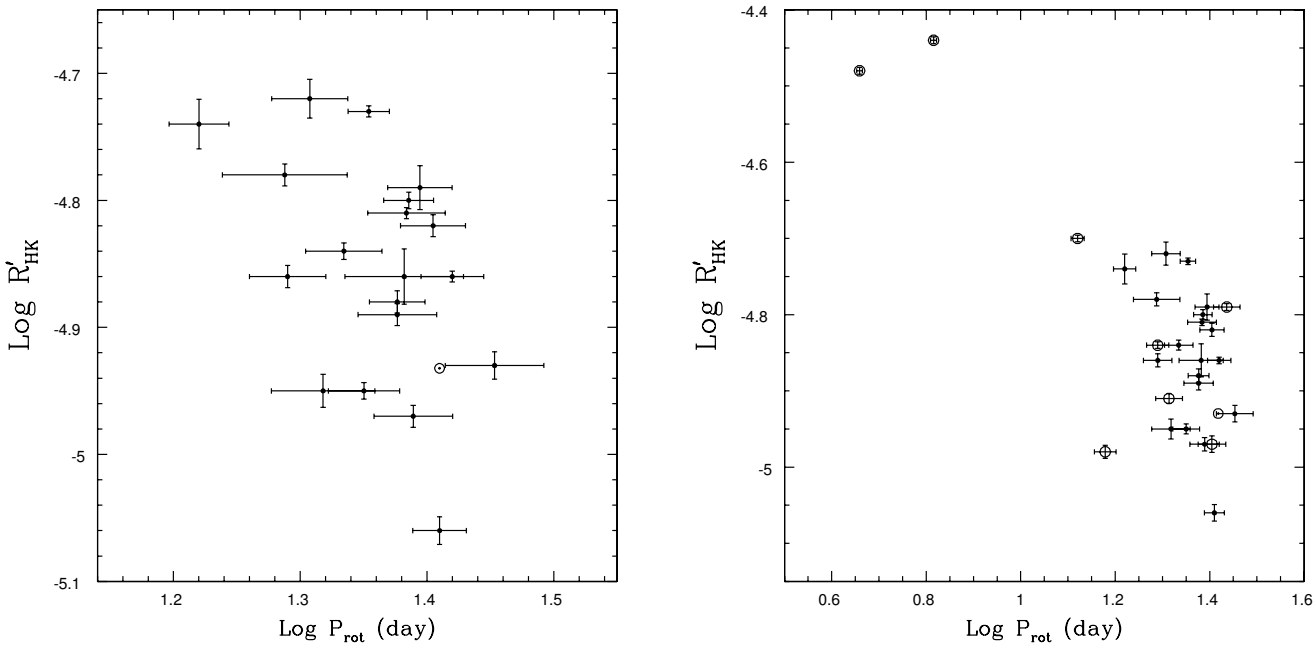

(a) (b)

Figure 4. The relationship between rotation period and an activity parameter for single (*left panel*) solar-type stars in M67. In the *right panel* we include binary systems represented by open circles. The position of the Sun at the rotation period corresponding to 25.4 days (Noyes et al. 1984) is indicated in both panels.

in the broad range of $\sim$ 20 – 30 days. Inspection of Figure 5 reveals that the mean level of activity of the Sun is less than that of most of the members (both single and binary) with measured rotation periods that are faster than the solar rotation. The spread of roughly a factor of two in $R'_{\rm HK}$ in this rotation regime exceeds the excursion of the full-disk K index in the Sun of $\sim$ 25% due to cycle modulation (Livingston et al. 2007). Paper I notes that the mean rms seasonal variation in HK index among the M67 solar-type stars exceeds that of the Sun by a factor of about 2.5. However, this would not be sufficient to entirely account for the range in $R'_{\rm HK}$, which must be due to other intrinsic properties related to the origin of magnetic field-related emission. We find from Table 1 a mean rotation period of 23.0 days $\pm$ 2.7 days for single solar-type stars while binaries exhibit a more rapid average rotation period of 15.4 days $\pm$ 8.5 days.

In order to further explore the origin of the empirical correlation in Figure 5, we construct the relation between $R'_{\rm HK}$ and Rossby number as shown in Figure 6. The Rossby number, which is defined here as the ratio of rotation period to global convective turnover time, is a hydrodynamic parameter that encapsulates two essential components of kinematic dynamos, namely, rotation and convection (Parker 1979, 1993). As before, we confine our consideration to single stars so as to avoid potential complexities that may involve binary membership as well as to compare results more directly to the Sun. We estimate the global convective turnover time in the Rossby number by linear interpolation of tabulated values as a function of stellar effective temperature given by Barnes & Kim (2010, see their Table 1), following the approach of Meibom et al. (2015).

We see in Figure 6 a general *increase* in activity to about a Rossby number of $\sim$ 0.9 – 1.0. Such a trend is contrary to what has been inferred in the case of the solar-type field stars in the Mt. Wilson Survey, where Noyes et al. (1984) found a tight anticorrelation between $R'_{\rm HK}$ and Rossby number. Their calculation of the Rossby number was based on a non-standard mixing length for the computation of the convective turnover time that minimized the dispersion in their $R'_{\rm HK}$–Rossby number relation (see Noyes et al. 1984, their Fig. 6). Other investigators have since found a similar anticorrelation with Rossby number based on different activity diagnostics and expanded samples of stars, including coronal X-ray emission (Pizzolato et al. 2003), Hα in field M dwarfs (Newton et al. 2017) and Ca II H and K in cluster members spanning an evolutionary range of ages (Mamajek & Hillenbrand 2008). The rotation periods found for the M67 solar-type stars are all similar and in

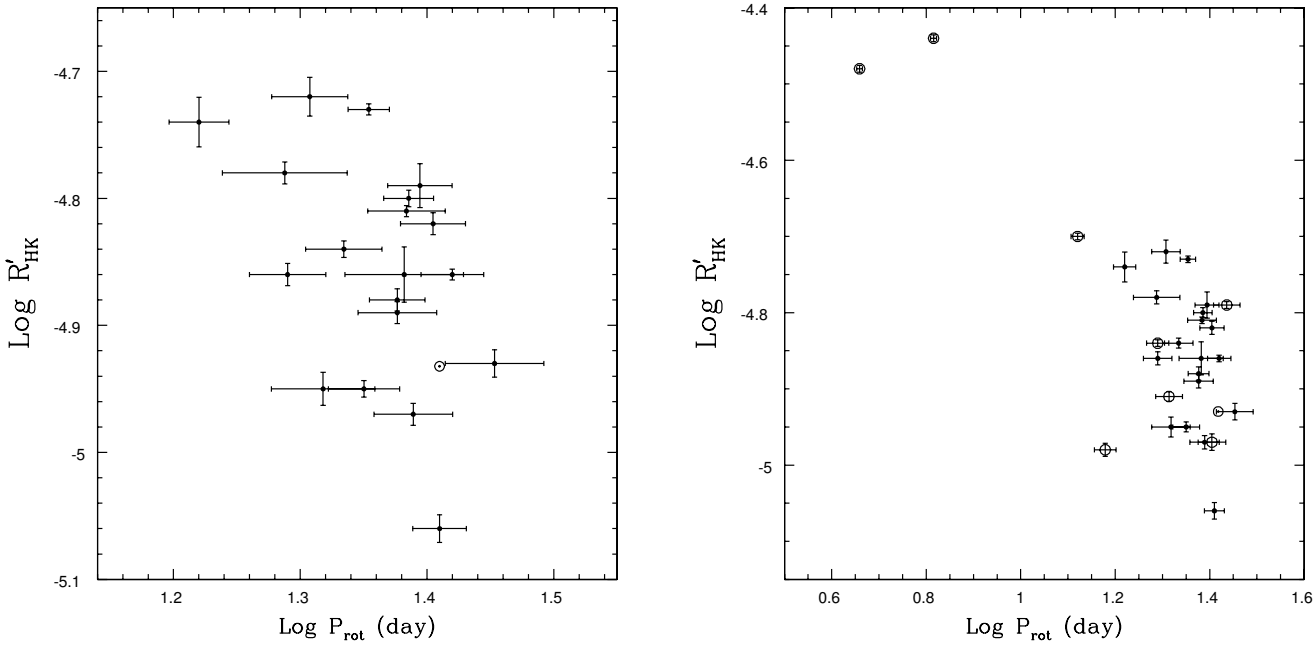

(a) (b)

Figure 5. The relationship between rotation period and an activity parameter for single (*left panel*) solar-type stars in M67. In the *right panel* we include binary systems represented by open circles. The position of the Sun at the rotation period corresponding to 25.4 days (Noyes et al. 1984) is indicated in both panels.

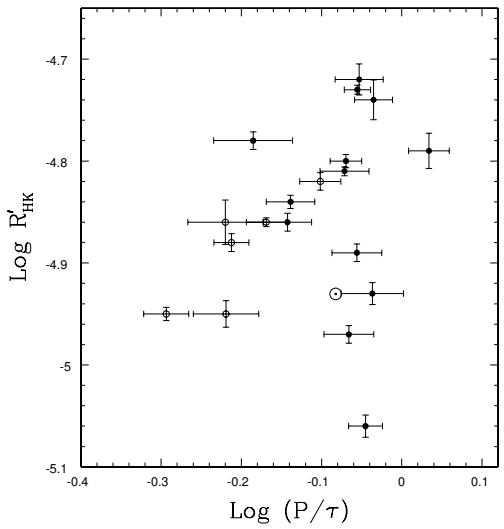

Figure 6. The relationship between normalized chromospheric activity and Rossby number for single solar-type stars in M67. The position of the Sun is indicated with the standard symbol. Open circles denote stars cooler than the Sun while filled circles represent stars warmer than the Sun.

the range of $\sim 20 - 26$ days while the convective turnover timescale spans a range of $\sim 18 - 44$ days. Therefore, we attribute the origin of the trend in Figure 6 to the variation of the characteristic time scale for global convection with effective temperature.This becomes more evident in Figure 7 where we plot Rossby number as a function of effective temperature. The declining trend reflects the dominance of the global convective time scale in determining the Rossby number for this particular sample. We further examine the correlation of activity with color in Figure 8 to find a decreasing trend that, in turn, implies a declining trend of activity with the temperature-dependent convective turnover time at the $\sim$ 4 Gyr age of these solar-type stars. In view of the general trend of declining activity with increasing rotation period, we display in Figure 9 the observed relation between rotation period and color. No obvious trend is apparent though the range of rotation period is relatively narrow.

4.2. *Stellar Ages from Chromospheric Activity and Gyrochronology*

With the advent of intensive investigations of planetary systems in the solar neighborhood, reliable age determinations for field stars become critical for an understanding of the evolution of exoplanet system architectures. The determination of stellar ages for field stars relies crucially on the calibration of age diagnostics based on open cluster observations. In this study we are specifically concerned with age estimates–and the dispersion

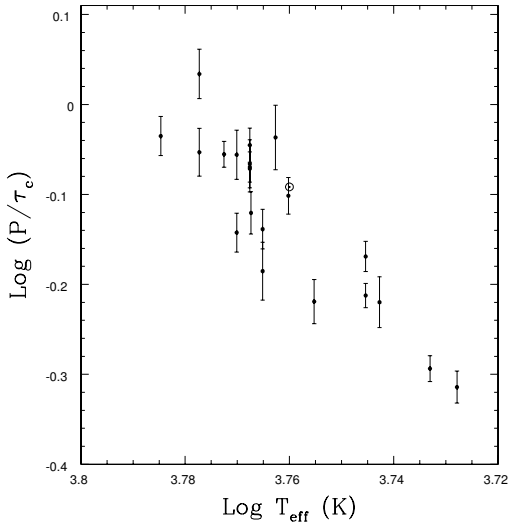

Figure 7. The Rossby number as a function of effective temperature for single cluster members only. The Sun is indicated.

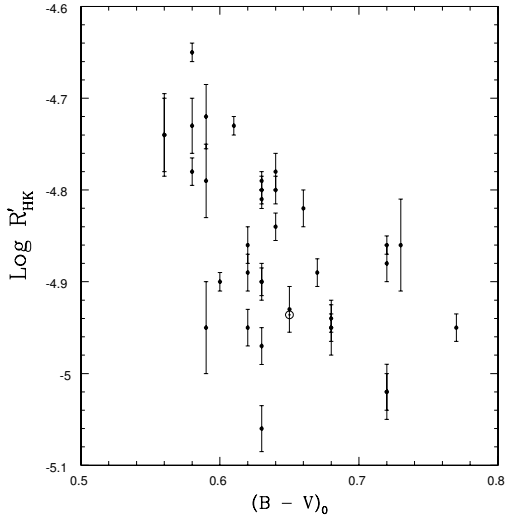

Figure 8. The trend of normalized chromospheric activity with color for the single solar-type cluster members for which we obtained H and K spectra.

in these estimates–based on correlations between chromospheric activity and age, and rotation frequency and age, respectively. Each of these is known to decrease with age (Skumanich 1972) and, hence, their calibration can lead to a useful tool for estimating the ages of individual stars in the field. We revisit the chromospheric age determinations in Paper I using our HK data given herein and the calibration of $R'_{\rm HK}$ with stellar age given by Mamajek & Hillenbrand (2008) for solar-type dwarfs, which is based on cluster data.

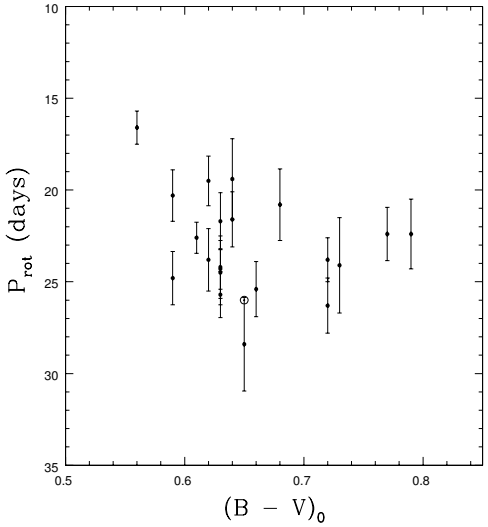

Figure 9. Rotation period as a function of color for single cluster members.

Our values of $R'_{\rm HK}$ from Table 2 – for single members only – inserted in the empirical relation determined by Mamajek & Hillenbrand (2008, their Equation 3) yields a mean chromospheric age for the ensemble of solar-type dwarfs in M67 of 4.54 ± 1.88 Gyr with an average random error in individual age determinations of ±0.34 Gyr. If we remove outliers with chromospheric ages less than 2 Gyr and greater than 7 Gyr then the average chromospheric age is 4.25 ± 1.37 Gyr. This mean age estimate is similar to that determined in Paper I, namely, 4.32 Gyr, based on an earlier age-activity calibration (Donahue 1998). For comparison, the mean chromospheric age of the Sun is approximately 4.3 Gyr though the range of cyclic variation of Ca II core emission can yield apparent chromospheric ages extending from about 2.5 Gyr (at solar maximum) to 6 Gyr for the Sun observed as a star at cycle minimum (Paper I).

Our rotation measures enable us to apply gyrochronology relations to infer ages based on rotation period, convective overturn time, and an assumed initial rotation period (Barnes 2010; Barnes & Kim 2010). In particular, we utilize Equation (32) in Barnes (2010) for the gyroage of the star where we adopt the initial period of 1.1 days for a calibrated solar model (Barnes 2010) and the tabulation of the global convective turnover timescale provided by Barnes & Kim (2010, their Table 1). Following Meibom et al. (2015), we retained the values of the constants in this relation as given by Barnes (2010). Again, using the rotation periods we find – for single members only–a mean gyroage of 4.15 Gyr ± 1.02 Gyr with an average error in the estimated gyroage of 1.14 Gyr, which is deduced from the errors in the individual

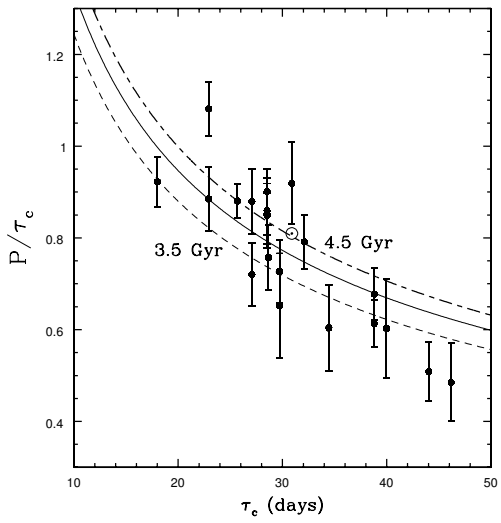

Figure 10. A least squares fit to Equation (2) at an age of 4.05 Gyr for the M67 single solar-type stars. The position of the Sun is shown. The dashed lines are calculated from Equation (2) for 3.5 and 4.5 Gyr, respectively.

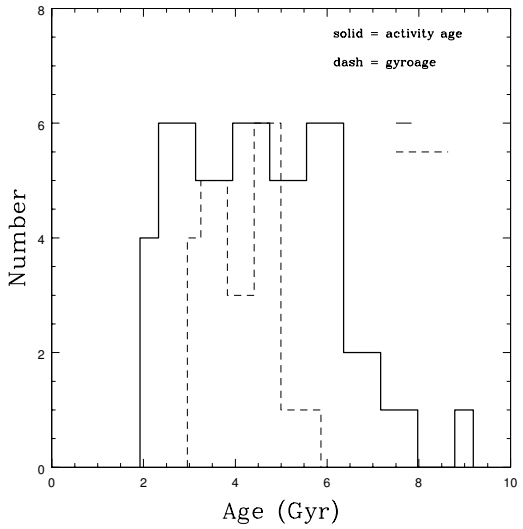

Figure 11. The distribution of apparent stellar ages for the single solar-type stars in M67. A chromospheric age based on $R'_{\rm HK}$ and, if a rotation measure is available, an age based on gyrochronology relations is determined. The average error bars in age for each kind of determination are shown.

rotation periods. Our mean gyroage is essentially identical to that determined by Barnes et al. (2016) though with a larger dispersion.

As a further consistency check, we apply the gyrochronological relation in the so-called I limit corresponding to Equation (9) in Barnes (2010). We rewrite this relation in terms of Rossby number as a function of global convective time scale at a given age since, as found by Noyes et al. (1984), the dispersion in relations involving the Rossby number appear to be minimized. This yields

$$Ro \;=\; \sqrt{\frac{P_0^2}{\tau^2} + \frac{2t}{k_{\rm I}\tau}} \quad , \qquad (1)$$

where Ro is the Rossby number, t is age in Myr, τ is the global convective turnover time in days (Barnes & Kim 2010), and k_I and P_0 are constants given by Barnes (2010). With $P_0 = 1.1$ days and $\tau \sim 10 - 30$ days, and at solar ages t $\sim 4 - 5$ Gyr, the first term in Equation (1) is much less than the second term. We therefore have to within a very good approximation that

$$Ro \;=\; \sqrt{\frac{2t}{k_{\rm I}\tau}} \quad . \qquad (2)$$

Performing a least-squares minimization of Equation (2) for the same single solar-type cluster members yields an age of t = 4.05 Gyr, or essentially identical to the mean gyroage we determined in the above. We plot this fit to the data in Figure 10 along with this same relation, for reference, at ages of 3.5 Gyr and 4.5 Gyr, respectively.

The mean chromospheric age and the mean age from gyrochronology agree to within their dispersions as well as to within their respective average errors based on the measurement errors in $R'_{\rm HK}$ and rotation period, respectively. The distribution of the apparent ages from both methods is illustrated in Figure 11. The chromospheric ages include all single solar-type stars with $R'_{\rm HK}$ values while the gyroage estimates, of course, are based only on those stars with rotation periods. Therefore, it is not surprising that the gyroage distribution in Figure 11 is more narrow than that for chromospheric ages, and that the mean gyroage is less than the mean chromospheric age: stars rotating at the solar rotation period or longer are not well represented.

We may compare the mean ages based on chromospheric activity and gyrochronology, respectively, with standard approaches to age determination in open clusters. Based on the observed color-magnitude diagram and theoretical isochrones from a variety of models, Yadav et al. (2008) concluded that the age of M67 is in the broad age range of 3.5 – 4.8 Gyr. Utilizing a spectroscopic analysis of the solar twin M67-1194 (S770), which also hosts a planet (Brucalassi et al. 2016), combined with evolutionary tracks yields an age estimate of 4.2 ± 1.6 Gyr for the cluster (Önehag et al. 2011). Sarajedini et al. (2009) applied theoretical isochrones to an analysis of deep 2MASS calibration photometry of M67 to determine an age range of 3.5 – 4.0 Gyr (also

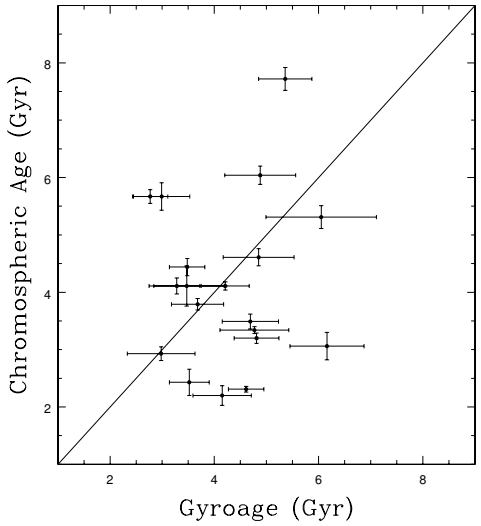

Figure 12. The correlation between chromospheric ages and ages determined from gyrochronology for single solar-type stars in M67. The solid line has unit slope.

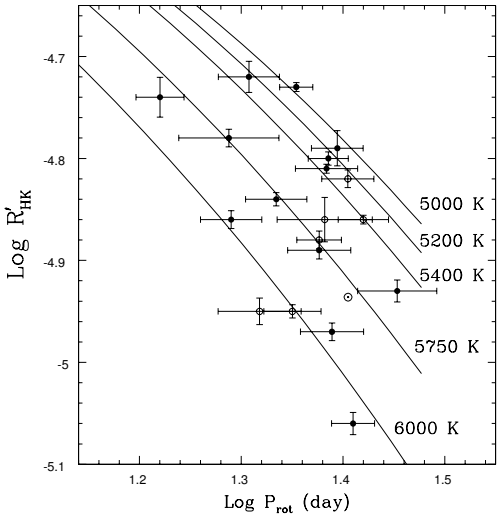

Figure 13. Chromospheric activity as a function of rotation period with curves of constant convective overturn time scale corresponding to the displayed effective temperatures. The curves are based on combining the empirical formula for chromospheric activity as a function of time from Mamajek & Hillenbrand (2008) and the theoretical model for rotational spindown given by Barnes (2010). Filled circles are stars warmer than the Sun while open circles represent stars cooler than the Sun.

see Bellini et al. 2010, who determine an age of 3.8 – 4.0 Gyr). Our inferred mean gyroage is closer to the upper range of this estimate while the mean chromospheric age is more similar to the determinations by Önehag et al. (2011) and the earlier study by Yadav et al. (2008), respectively.

We compare in Figure 12 the results from these two approaches for those single members that have both $R'_{\rm HK}$ and rotation period measurements, respectively. Inspection of Figure 12 reveals that the line of unit slope divides the sample into stars that are more chromospherically active for their gyroage (i.e., they appear younger chromospherically at their rotation period) while those stars above the line are less active (i.e., older activity age) for their gyrochronological age. The scatter about the line is reflected in the relative dispersions in the histogram in Figure 11.

5. DISCUSSION

We consider the implications and interpretation of the results for the relationship between activity, rotation and convection in solar-type stars at approximately solar age. We reformulate Figure 5 (rotation period vs. $R'_{\rm HK}$) by comparing the results to a semi-empirical relationship between rotation and activity derived as follows. We utilize the gyrochronology relation in Barnes (2010, Equation 32) for a given rotation period and (global) convective overturn timescale, calculate the resulting age and use this apparent age in the log $R'_{\rm HK}$ – log t empirical calibration given by Mamajek & Hillenbrand (2008, their Equation 4). This yields the curves in Figure 13 denoted by the stellar effective temperatures that correspond to the convective overturn times from Barnes & Kim (2010). The apparent scatter among the stars with $R'_{\rm HK}$ values within a factor of two of the mean solar value now appears more ordered along contours of constant convective overturn time scales. However, individual stars in Figure 13 do not necessarily have effective temperatures that correspond to the curves near which they appear, suggesting that the object is either overactive or underactive at a given rotation period. We infer from Figure 13 that the *ensemble* of solar-type stars in M67 is consistent with the Barnes & Kim (2010) model for rotational evolution combined with the empirical calibration of activity and age determined by Mamajek & Hillenbrand (2008) though this is not necessarily the case on a star-by-star basis. In particular, our inspection of the underlying data in Figure 13 reveals that, of the 11 objects with effective temperatures $\gtrsim$ 5800 K, eight of them have values of $R'_{\rm HK}$ that are above the curve corresponding to $T_{\rm eff}$ = 5750 K. In other words, these stars that are $\sim$ 100 K warmer than the Sun exhibit enhanced chromospheric emission for their rotation period and cluster member age. This is reminiscent of the result by van Saders et al. (2016) suggesting the onset of a reduced efficiency of magnetic braking, particularly in late-type dwarfs warmer than the Sun.

We further consider this from the perspective of apparent ages derived from chromospheric activity and gyrochronolgy, respectively, for the single solar-type members. We display in Figure 14 chromospheric age as a function of color, again for the single members only. Inspection of Figure 14 reveals that stars warmer than the Sun exhibit activity ages younger than 4 Gyr. By about the solar color there is an increasing spread in chromospheric ages older than about 4 Gyr. Thus, these warmer stars exhibit enhanced activity for their cluster age while cooler stars are characterized by comparatively lower activity at the age of M67. An analgous plot but for gyrochronological ages is given in Figure 15 where trends are less apparent except that stars later than the Sun tend to be rotating faster than the cluster age. We cannot exclude detection biases in the results for Figure 15, which may act toward enhanced detection of rotational modulation at later spectral types and the absence of rotation measures for solar-type rotation periods or longer.

In summary, we find that the mean ages for the single members based on gyrochronology and chromospheric activity-age calibrations are consistent with each other, and other methods, to within the errors. However, the large spread $\sim 25\%$ in age estimates for a presumably coeval population serves as a caution for the application of these techniques to individual stars. Finally, we note that Curtis (2017) has argued that interstellar extinction could have an impact on moderate-resolution chromospheric H and K measures in M67. If this applies uniformly across the cluster, then we make a preliminary estimate that our intrinsic HK fluxes should be approximately 9% higher to account for this extra component of extinction. Increasing our $R'_{\rm HK}$ values accordingly yields a mean chromospheric age estimate for M67 of about 3.9 Gyr $\pm$ 1.1 Gyr, or within 6% of the mean gyroage. However, the latter is biased towards single members with rotation measures. Those without rotation measurements could be rotating more slowly with modulation amplitudes below the level of detection. If this is the case then the mean gyroage found here is a minimum value.

In the context of dynamo models, we adopt the relation given by Brandenburg et al. (2017, their Equation 11) to calculate the residual c as a function of the activity parameter $R'_{\rm HK}$ for single stars only. According to Brandenburg et al. (2017), this residual, which is plotted in Figure 16, should be constant if there are no other dependences, which does indeed appear to be the case for the Mt. Wilson survey stars. The best fit line to the data (not including the Sun) is shown. By contrast, this quantity for the M67 sample exhibits a clear and increasing trend with activity in Figure 16, suggesting the presence of a systematic dependency on another quantity. The fit shown here, in the terminology of Brandenburg et al. (2017), is characterized by constants $\rho = 1.25$ and $\log c_1 = 1.11$.

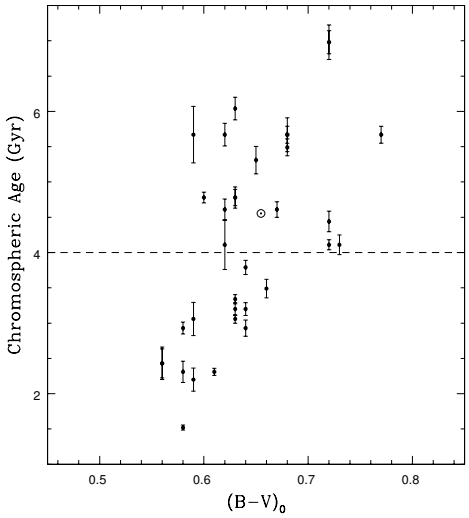

Figure 14. Chromospheric age as a function of intrinsic $B-V$ color for single solar-type stars in M67. A horizontal dashed line is drawn at 4 Gyr. Note that warmer stars appear at younger apparent chromospheric ages while stars more similar to the Sun in color exhibit a dispersion of apparent ages though most exceed 4 Gyr.

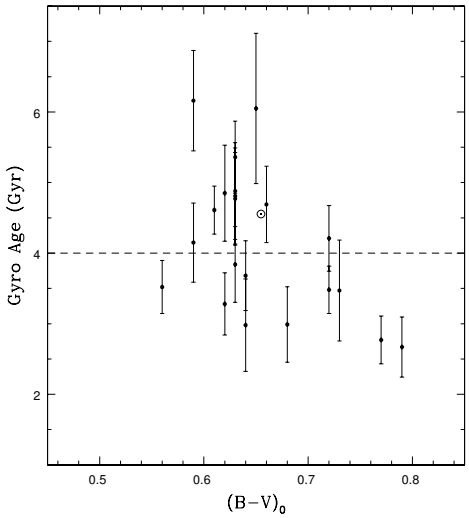

Figure 15. Gyroages as a function of $B-V$ color for single solar-type stars in M67. The horizontal dashed line divides the diagram into stellar gyroages > 4 Gyr and < 4 Gyr. The stars cooler than the Sun appear preferentially at gyroages < 4 Gyr.

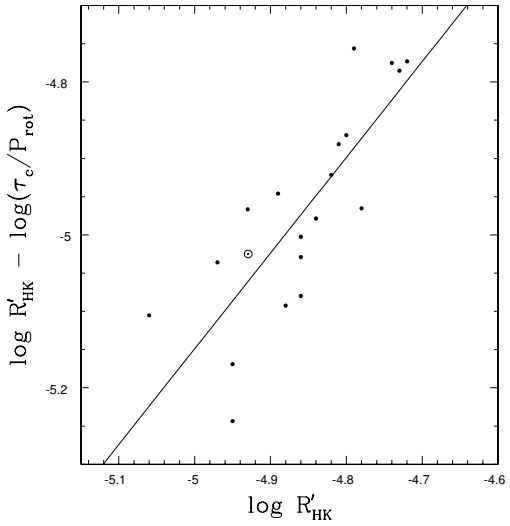

Figure 16. The residual log $R'_{HK} - \log(\tau/P_{rot})$ versus log R'_{HK} for the single M67 solar-type stars with determined rotation periods. The trend suggests an additional systematic dependency of activity on another parameter. The position of the Sun is shown based on observational data given by Noyes et al. (1984) but with the convective turnover time interpolated from model data provided by Barnes & Kim (2010). The best fit line to the data (not including the solar point) is displayed.

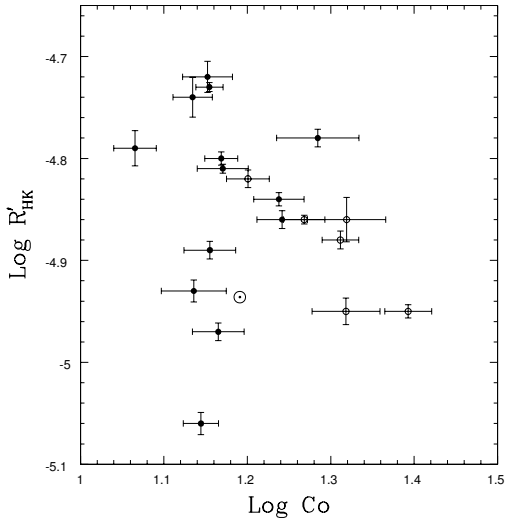

Figure 17. Relative chromospheric activity as a function of Coriolis number. The declining branch of this diagram suggests the presence of stars with antisolar differential rotation and a corresponding increase in importance of the small-scale magnetic flux relative to the large-scale field. Open circles represent stars cooler than solar and filled circles denote objects warmer than solar.

Considering further the relation in displayed in Figure 16, it can be shown that, for similar rotation periods, the slope of the line, ρ, is approximately given by

$$\rho = 1 - \frac{d\tau_c/dT_{\rm eff}}{dR'_{\rm HK}/dT_{\rm eff}} \frac{R'_{\rm HK}}{\tau_c} \quad . \tag{3}$$

Given that $R'_{\rm HK}$ is observed to decrease with color (Figure 8) and the global convective time scale increases toward later types, the second term in (3) is < 0. Hence, $\rho > 1$, which accounts for the relatively steep slope of the relation in Figure 16. From a physical perspective, stellar effective temperature and perhaps the associated convective properties are key parameters in governing magnetic field-related activity for this homogeneous sample (in age and metallicity) of solar-type stars with similar rotation periods at their cluster age $\sim$ 4 Gyr.

The surface magnetic flux itself not only depends on convection and rotation but the strength of the large-scale magnetic field may depend on the nature of any *differential* rotation that is present. Karak et al. (2015) developed simulations in which they examined field properties in solar-type stars, for example, as functions of the Coriolis number and the sense of differential rotation, i.e., solar or antisolar, that may be present. Given that the surface magnetic flux is proportional in some way to the activity parameter, $R'_{\rm HK}$, we compare our observed relation with Coriolis number, defined in Figure 17 as Co = $4\pi\tau_c/P$, where τ_c and P are the convective time scale and rotation period, respectively. This is essentially equivalent to Figure 6 but using inverse Rossby number times a constant factor. Nevertheless, we retain this Figure here because the displayed observational results can then be more readily compared to the results from computational models that utilize Coriolis number, as discussed below.

We see in Figure 17 a decline in normalized activity with increasing Coriolis number primarily in the region where log $R'_{\rm HK} \gtrsim$ -4.9. In the Karak et al. (2015, see their Figure 12b) models, a similar trend is seen in their calculation of the mean magnetic field strength but for stars characterized by *antisolar* differential rotation, i.e., rotation frequency increasing from equator to poles rather than, as in the Sun, faster equatorial rotation that then declines polewards. Our results in Figure 17 are suggestive but unverified with respect to the sense of any differential rotation, the detection of which would typically require a much longer time series so that the reality of any apparent drifts in rotation period could be confirmed. However, the sign of the latitudinal gradient would be difficult to ascertain.

6. CONCLUSIONS

In the single solar-type stars in M67 in which we are able to measure modulation in their respective $K2$ light curves, we find rotation periods generally in the range $\sim 20 - 25$ days, or about 10% – 20% faster than the solar rotation period. The sample exhibits a general decline of activity with increasing rotation period in this relatively narrow range of rotation periods. However, we see an increase of activity with Rossby number, which we attribute primarily to the broader range of convective overturn time within this relatively narrow range of rotation periods. The normalized chromospheric emission exhibits a declining trend with effective temperature suggesting that as convective energy decreases so too does the magnetic field-related activity.

The gyrochronological and chromospheric ages, respectively, are of $\sim 4 - 4.5$ Gyr, which is consistent with analyses based on isochrones. However, stars warmer than the Sun exhibit both enhanced emission for their effective temperature and cluster age, consistent with the onset of a reduced efficiency of magnetic braking (van Saders et al. 2016). This, in turn, could arise from a transition in dominance from large-scale fields to small-scale fields by the age of M67. The presence of single solar-type stars with gyrochronological ages that differ significantly from the solar-like age of M67 emphasizes the complex nature of angular momentum evolution in solar-type stars.

Finally, the forthcoming $K2$ *Campaign* 16 will yield additional observations of M67 cluster members with high-precision photometry that can be compared with, and extend, the extant $K2$ data from *Campaign* 5. We also intend to pursue further spectroscopic investigations but at echelle resolutions utilizing large-aperture telescopes with multi-object spectrographs in order to obtain high quality data in the faint cores of the Ca II H and K cores. This will enable us to improve the accuracy of the measurements of chromospheric emission while also examining quantitatively the potential effects of interstellar extinction. These additional data will enable an even deeper investigation of the complex relationships between rotation, convection properties, and angular momentum evolution near the age of the Sun.

We gratefully acknowledge the skilled assistance of WIYN telescope operators Dave Summers and Doug Williams. The assistance of D. Harmer at setup at WIYN was very much appreciated. We also thank G. Basri for sharing his preliminary findings in advance of publication. One of us (MSG) acknowledges very helpful discussions with R. Komm and J. Harvey on the wavelet transform of a time series. We acknowledge partial support of this investigation by grants to AURA/NSO from, respectively, the NASA *Kepler*/$K2$ Guest Observer program through Agreement No. NNX15AV53G and from the NN-EXPLORE program through JPL RSA 1533727, which is administered by the NASA Exoplanet Science Institute (NExScI).

Table 1. Activity and Rotation Period Measurements

Sanders No. (1)	$(B-V)_0$ (2)	HK (mÅ) (3)	Error (mÅ) (4)	Period (days) (5)	Error (days) (6)	Binarity[a] (7)
603	0.55	208	9.99	16.6	1.8	SM
621	0.62	292	3.57	—	—	SB1
724	0.63	216	2.55	—	—	SM
746	0.67	200	3.30	—	—	SM
747	0.66	378	4.57	7.01	0.25	SB2
747	0.66	378	4.57	6.08	0.13	SB2
770	0.64	215	4.03	—	—	SM
777	0.63	190	2.30	—	—	SM

Table 1 continued

Table 1 *(continued)*

Sanders No.	$(B-V)_0$	HK (mÅ)	Error (mÅ)	Period (days)	Error (days)	Binarity[a]
(1)	(2)	(3)	(4)	(5)	(6)	(7)
779	0.65	190	8.34	—	—	SM
785	0.66	214	4.59	25.4	3.0	SM
789	0.62	218	2.94	—	—	SB2
801	0.68	188	5.12	20.8	3.9	SM
802	0.68	187	2.57	—	—	SM
829	0.59	172	7.49	—	—	SM
942	0.59	193	2.22	19.5	2.1	SB1
943	0.72	188	4.93	25.4	3.4	SB1
945	0.63	213	3.97	24.3	2.2	SM
951	0.68	204	3.97	—	—	SB1
958	0.62	191	3.51	23.8	3.4	SM
963	0.67	195	3.13	20.6	2.7	SB1, 90.28
965	0.72	215	2.84	26.3	3.0	SM
966	0.63	—	—	21.7	3.1	SM
969	0.63	162	3.10	25.7	2.5	SM
981	0.67	190	2.21	—	—	SB2, 56.0
982	0.56	231	6.99	—	—	SB1, 373
991	0.64	205	3.70	21.6	3.0	SM
996	0.85	—	—	6.10	0.08	BM
1004	0.72	178	3.34	—	—	SM
1012	0.70	196	2.47	—	—	SB1, 641
1014	0.67	238	3.85	—	—	SB2, 16.2
1033	0.57	209	8.69	—	—	SM
1041	0.69	193	9.51	—	—	SM
1048	0.65	150	2.08	—	—	SM
1050	0.62	355	4.51	—	—	SB1
1064	0.62	213	2.06	27.3	3.5	SB1,575
1065	0.76	202	5.21	—	—	SB1, 150
1078	0.62	179	2.87	—	—	SM
1087	0.60	183	2.09	—	—	SM
1089	0.63	177	3.14	24.5	3.5	SM
1095	0.61	229	2.58	22.6	1.7	SM
1096	0.62	197	3.91	19.5	2.7	SM
1106	0.65	187	4.03	28.4	5.1	SM
1112[b]	0.74	536	8.31	2.64	0.04	BLM, SB1, 2.65[b]

Table 1 continued

Table 1 *(continued)*

Sanders No. (1)	$(B-V)_0$ (2)	HK (mÅ) (3)	Error (mÅ) (4)	Period (days) (5)	Error (days) (6)	Binarity[a] (7)
1112[b]	0.74	536	8.31	2.90	0.08	BLM , SB1, 2.65[b]
1208	0.78	228	4.53	—	—	SB2, 19.9
1212	0.73	218	13.1	24.7	5.2	SM
1218	0.64	222	4.34	19.4	4.4	SM
1247	0.58	226	3.12	13.2	0.84	SB2, 69.8
1248	0.58	242	2.42	—	—	SM
1249	0.74	187	3.51	15.1	1.6	SB1
1251	0.71	245	3.43	—	—	SB1
1252	0.59	201	8.14	20.3	2.8	SM
1255	0.63	210	2.39	24.2	3.4	SM
1258	0.63	190	3.59	—	—	SM
1260	0.58	204	3.36	—	—	SM
1269	0.72	177	4.75	—	—	SM
1278	0.73	181	11.9	—	—	SB2
1289	0.72	209	4.68	23.8	2.4	SM
1307	0.77	195	3.56	22.4	2.9	SM
1309	0.79			22.4	3.8	SM
1318	0.58	217	7.05	—	—	SM
1420	0.59	205	8.29	24.8	2.9	SM
1449	0.62	152	3.17	—	—	SM
1452	0.63	339	3.83	4.56	0.08	SB1
1462	0.63	177	1.86	—	—	SB1
1477	0.68	191	2.43	—	—	SM

[a] From Geller et al. (2015) using their designations for membership and binarity. SM represents a single cluster member; BM is a binary member and BLM denotes a likely binary member. Orbital periods in days quoted from Paper I.

[b] HY Cnc: *ROSAT* X-ray source classified as RS CVn system (Belloni et al. 1998). This extreme object is not included in our analysis of chromospheric activity in M67. Our periodogram analysis yields two periods listed here as separate entries. An orbital period is cited by Mooley & Singh (2015).

Table 2. Activity Parameters and Age Estimates

Sanders No.	T_{eff} (°K)	R'_{HK}	Error	Global τ_c[a] (days)	Chromospheric Age[b] (Gyr)	Error (Gyr)	Gyrochronological Age[c] (Gyr)	Error (Gyr)	Binarity[d]
(1)	(2)	(3)	(4)	(5)	(6)	(7)	(8)	(9)	(10)
603	6091.	1.82E-05	1.62E-06	18.00	2.43	0.46	3.52	0.75	SM
621	5890.	2.74E-05	5.06E-07	27.07	—	—	—	—	BM
724	5856.	1.62E-05	3.53E-07	28.52	3.06	0.12	—	—	SM
746	5725.	1.28E-05	4.16E-07	33.25	4.61	0.22	—	—	SM
747	5757.	3.61E-05	5.91E-07	32.09	—	—	—	—	BM
770	5823.	1.57E-05	5.45E-07	29.72	3.20	0.18	—	—	SM
777	5856.	1.26E-05	3.20E-07	28.52	4.78	0.23	—	—	SM
785	5757.	1.50E-05	5.94E-07	32.09	3.49	0.26	4.69	1.08	SM
789	5890.	1.68E-05	4.17E-07	27.07	—	—	—	—	BM
801	5692.	1.12E-05	6.32E-07	34.45	5.67	0.48	2.99	1.07	SM
802	5692.	1.12E-05	3.17E-07	34.45	5.67	0.24	—	—	SM
829	5988.	1.11E-05	1.14E-06	22.94	5.67	0.80	—	—	SM
942	5991.	1.44E-05	3.38E-07	22.81	—	—	—	—	BM
943	5564.	1.08E-05	5.55E-07	38.81	—	—	—	—	BM
945	5856.	1.58E-05	5.51E-07	28.52	3.20	0.18	4.81	1.36	SM
951	5692.	1.31E-05	4.89E-07	34.45	—	—	—	—	BM
958	5890.	1.30E-05	4.98E-07	27.07	4.61	0.30	4.85	1.36	SM
963	5725.	1.22E-05	3.96E-07	33.25	—	—	—	—	BM
965	5564.	1.39E-05	3.20E-07	38.81	4.11	0.14	4.21	0.93	SM
966	5853.	1.00E-11	1.00E-12	28.65	0.01	0.01	3.84	1.07	SM
969	5856.	8.73E-06	4.30E-07	28.52	7.72	0.40	5.36	1.02	SM
981	5725.	1.17E-05	2.79E-07	33.25	—	—	—	—	BM

Table 2 continued

Table 2 *(continued)*

Sanders No.	T_{eff}	R'_{HK}	Error	Global τ_c[a]	Chromospheric Age[b]	Error	Gyrochronological Age[c]	Error	Binarity[d]
	(°K)			(days)	(Gyr)	(Gyr)	(Gyr)	(Gyr)	
(1)	(2)	(3)	(4)	(5)	(6)	(7)	(8)	(9)	(10)
991	5823.	1.44E-05	5.01E-07	29.72	3.79	0.20	3.68	0.99	SM
996	5165.	1.00E-11	1.00E-12	52.09	—	—	—	—	BM
1004	5564.	9.56E-06	3.75E-07	38.81	6.98	0.33	—	—	SM
1012	5628.	1.20E-05	2.92E-07	36.64	—	—	—	—	BM
1014	5725.	1.76E-05	4.87E-07	33.25	—	—	—	—	BM
1033	6091.	1.83E-05	1.41E-06	18.00	2.43	0.41	—	—	SM
1048	5790.	6.75E-06	2.76E-07	30.90	9.59	0.26	—	—	SM
1050	5890.	3.63E-05	6.40E-07	27.07	—	—	—	—	BM
1064	5890.	1.61E-05	2.93E-07	27.07	—	—	—	—	BM
1065	5439.	1.20E-05	5.35E-07	43.02	—	—	—	—	BM
1078	5890.	1.13E-05	4.07E-07	27.07	5.67	0.32	—	—	SM
1087	5957.	1.25E-05	3.10E-07	24.24	4.78	0.15	—	—	SM
1089	5856.	1.07E-05	4.36E-07	28.52	6.04	0.32	4.88	1.37	SM
1095	5923.	1.88E-05	3.75E-07	25.67	2.31	0.10	4.61	0.68	SM
1096	5890.	1.39E-05	5.55E-07	27.07	4.11	0.70	3.28	0.88	SM
1106	5790.	1.17E-05	5.33E-07	30.90	5.31	0.39	6.05	2.13	SM
1208	5378.	1.44E-05	4.43E-07	45.04	—	—	—	—	BM
1212	5530.	1.39E-05	1.44E-06	39.98	4.11	0.28	3.47	1.43	SM
1218	5823.	1.66E-05	5.89E-07	29.72	2.93	0.23	2.98	1.31	SM
1247	6025.	1.99E-05	4.85E-07	21.29	—	—	—	—	BM
1248	6025.	2.25E-05	3.78E-07	21.29	1.52	0.07	—	—	SM
1249	5501.	1.05E-05	3.77E-07	40.98	—	—	—	—	BM
1251	5596.	1.74E-05	3.95E-07	37.72	—	—	—	—	BM
1252	5988.	1.92E-05	1.38E-06	22.94	2.20	0.33	4.15	1.12	SM
1255	5856.	1.53E-05	3.32E-07	28.52	3.34	0.13	4.77	1.31	SM

Table 2 continued

Table 2 *(continued)*

Sanders No.	T_{eff} (°K)	R'_{HK}	Error	Global τ_c[a] (days)	Chromospheric Age[b] (Gyr)	Error (Gyr)	Gyrochronological Age[c] (Gyr)	Error (Gyr)	Binarity[d]
(1)	(2)	(3)	(4)	(5)	(6)	(7)	(8)	(9)	(10)
1258	5856.	1.26E-05	4.99E-07	28.52	4.78	0.30	—	—	SM
1260	6025.	1.65E-05	5.24E-07	21.29	2.93	0.17	—	—	SM
1269	5564.	9.55E-06	5.36E-07	38.81	6.98	0.49	—	—	SM
1289	5564.	1.32E-05	5.28E-07	38.81	4.44	0.29	3.48	0.67	SM
1307	5408.	1.13E-05	3.58E-07	44.04	5.67	0.24	2.77	0.68	SM
1309	5344.	1.00E-11	1.00E-12	46.18	0.01	0.01	2.67	0.85	SM
1318	6022.	1.85E-05	1.10E-06	21.44	2.31	0.30	—	—	SM
1420	5988.	1.61E-05	1.26E-06	22.94	3.06	0.47	6.16	1.42	SM
1449	5890.	7.40E-06	4.50E-07	27.07	8.96	0.43	—	—	SM
1452	5856.	3.33E-05	5.32E-07	28.52	—	—	—	—	BM
1462	5856.	1.07E-05	2.57E-07	28.52	—	—	—	—	BM
1477	5692.	1.16E-05	3.00E-07	34.45	5.49	0.24	—	—	SM

[a] Global convective overturn time interpolated from Table 1 in Barnes & Kim (2010).

[b] From empirical $R'_{\rm HK}$–age relation given by Mamajek & Hillenbrand (2008), their Equation (3).

[c] Inferred from rotation period data in Table 1, the global τ_c in column (5) and the rotational evolution model corresponding to Equation (32) in Barnes (2010).

[d] Binarity data from Geller et al. (2015). See Table 1 notes for meaning of entries.

REFERENCES

Aigrain, S., Parviainen, H., & Pope, B. J. S. 2016, MNRAS, 459, 2408

Baliunas, S. L., Donahue, R. A., Soon, W. H., et al. 1995, ApJ, 438, 269

Barnes, S. A. 2010, ApJ, 722, 222

Barnes, S. A., & Kim, Y.-C. 2010, ApJ, 721, 675-685

Barnes, S. A., Weingrill, J., Fritzewski, D., Strassmeier, K. G., & Platais, I. 2016, ApJ, 823, 16

Bellini, A., Bedin, L. R., Piotto, G., et al. 2010, A&A, 513, A50

Belloni, T., Verbunt, F., & Mathieu, R. D. 1998, A&A, 339, 431

Bloomfield, P. 1976, Fourier Analysis of Time Series: An Introduction, 1st Edition (New York, John Wiley & Sons, Inc.)

Brandenburg, A., Mathur, S., & Metcalfe, T. S. 2017, ApJ, 845, 79

Brucalassi, A., Pasquini, L., Saglia, R., et al. 2016, A&A, 592, L1

Curtis, J. L. 2017, AJ, 153, 275

Donahue, R. A. 1998, Cool Stars, Stellar Systems, and the Sun, 154, 1235

Eberhard, G., & Schwarzschild, K. 1913, ApJ, 38, 292

Geller, A. M., Latham, D. W., & Mathieu, R. D. 2015, AJ, 150, 97

Giampapa, M. S., Hall, J. C., Radick, R. R., & Baliunas, S. L. 2006, ApJ, 651, 444 (Paper I)

Giampapa, M. S. 2016, IAU Focus Meeting, 29, 365

Gonzalez, G. 2016a, MNRAS, 459, 1060

Gonzalez, G. 2016b, MNRAS, 463, 3513

Hall, J. C., & Lockwood, G. W. 1995, ApJ, 438, 404

Howell, S. B., Sobeck, C., Haas, M., et al. 2014, PASP, 126, 398

Karak, B. B., Käpylä, P. J., Käpylä, M. J., et al. 2015, A&A, 576, A26

Kraft, R. P. 1967, ApJ, 150, 551

Linsky, J. L., McClintock, W., Robertson, R. M., & Worden, S. P. 1979, ApJS, 41, 47

Livingston, W., Wallace, L., White, O. R., & Giampapa, M. S. 2007, ApJ, 657, 1137

Lockwood, G. W., Skiff, B. A., Henry, G. W., et al. 2007, ApJS, 171, 260

Lovis, C., & Fischer, D. 2010, Exoplanets, 27

Mamajek, E. E., & Hillenbrand, L. A. 2008, ApJ, 687, 1264-1293

Meibom, S., Barnes, S. A., Platais, I., et al. 2015, Nature, 517, 589

Mooley, K. P., & Singh, K. P. 2015, MNRAS, 452, 339

Morris, B. M., Hawley, S. L., Hebb, L., et al. 2017, ApJ, 848, 58

Newton, E. R., Irwin, J., Charbonneau, D., et al. 2017, ApJ, 834, 85

Noyes, R. W., Hartmann, L. W., Baliunas, S. L., Duncan, D. K., & Vaughan, A. H. 1984, ApJ, 279, 763

Önehag, A., Korn, A., Gustafsson, B., Stempels, E., & Vandenberg, D. A. 2011, A&A, 528, A85

Parker, E. N. 1979, Oxford, Clarendon Press; New York, Oxford University Press

Parker, E. N. 1993, ApJ, 408, 707

Pizzolato, N., Maggio, A., Micela, G., Sciortino, S., & Ventura, P. 2003, A&A, 397, 147

Press, W. H., & Rybicki, G. B. 1989, ApJ, 338, 277

Reiners, A., & Giampapa, M. S. 2009, ApJ, 707, 852

Rottman, G. 2005, SoPh, 230, 7

Rottman, G. 2006, SSRv, 125, 39

van Saders, J. L., Ceillier, T., Metcalfe, T. S., et al. 2016, Nature, 529, 181

Sarajedini, A., Dotter, A., & Kirkpatrick, A. 2009, ApJ, 698, 1872

Shapiro, A. I., Solanki, S. K., Krivova, N. A., Yeo, K. L., & Schmutz, W. K. 2016, A&A, 589, A46

Skumanich, A. 1972, ApJ, 171, 565

Solanki, S. K., & Unruh, Y. C. 2013, Astronomische Nachrichten, 334, 145

Taylor, B. J. 2007, AJ, 133, 370

Torrence, C., & Compo, G. P. 1998, Bull. Amer. Meteor. Soc., 79, 62

Wilson, O. C. 1966, Science, 151, 1487

Yadav, R. K. S., Bedin, L. R., Piotto, G., et al. 2008, A&A, 484, 609